Relativity and Timing in X-ray Pulsar Navigation†

N. Ashby
University of Colorado
Boulder, Colorado, USA 80305

D. A. Howe
National Inst. of Standards and Tech.
Boulder, Colorado, USA 80305

***Abstract*—XNAV is a technology demonstration involving many organizations that will use photons from X-ray pulsars for navigation and spacecraft attitude determination. This paper summarizes relativistic effects in the context of XNAV. It also characterizes the primary task in the time domain of realizing an on-board master clock that time-tags detected X-ray photons with sufficient accuracy to permit meaningful navigation solutions. XNAV must first estimate the periods of uncatalogued X-ray pulsars to determine suitable candidate pulsars for navigation. This task will use an efficient search algorithm to determine the pulsar period from a sensor aimed at the pulsar.**

As a part of this search and catalogue task, an accumulator that integrates photon counts will compute average counts per sampling time interval, in time bins that are small compared to the pulsar's period. This operation is dubbed the pulsar profiler function. It is intended to build a reference or standard profile of a chosen pulsar for later use. The search and catalogue need to be sufficient for navigation based on times-of-arrival of pulsar signals in real time *vs.* the on-board reference clock. Operationally, the timing module locates in time the highest peak (or other defined phase center) in the group velocity of received, periodic plane-wave pulses from catalogued pulsars. The goal is to permit navigation accuracy approaching 100 m. This will be accomplished by cross-correlation of catalogued profiles to incoming profiles based on X-ray sensor data collected in real time.

1. Introduction

In deep space where GPS is not available, studies of navigation scenarios using periodic signals from pulsars are of great interest [1],[2],[3]. XNAV is a project intended to demonstrate that spacecraft attitude, position and velocity can be determined to about 100 m accuracy with X-ray signals from distant pulsars. In the X-ray region of the spectrum, pulsar signals are usually quite weak. Long observation times may be required and that entails disentangling spacecraft motion during the observations from the measurements themselves in order to perform accurate navigation. Time stability over these long times together with Poisson statistics of photon counting of weak signals impose restrictions on navigation accuracy. In contrast, pulsar radio signals do not usually suffer from such counting noise.

In Section 2 we discuss the processes involved in navigation using pulsar signals. Section 3 discusses the effect of white frequency clock noise, modeled in terms of random walk in time, on time-tagging and subsequent time-binning for on-board processing of photon times-of-arrival data. It is shown that if a good atomic clock such as a Rubidium Atomic Frequency Standard (RAFS), or a Cesium standard, is used to time-tag the individual arriving photons, then, for most pulsars, errors arising from intrinsic clock noise are substantially lower than errors arising from Poisson counting statistics. In Section 4 we discuss some of the relativistic effects that must be accounted for.

†Contribution of the U. S. government and sponsored by the Defense Advanced Research Projects Agency. Article is not subject to copyright.

2. Navigation with pulsar signals

X-rays are useful for navigation for many reasons. First, they do not suffer interstellar dispersion so the electron content along the photon path does not need to be known. Secondly, X-ray detectors can be made small compared to radio telescopes and so could potentially be useful in a space vehicle. Central to this project is the fact that the periods of pulsars have very good stability (except for occasional anomalies due to starquakes and other events), and predictable higher period derivatives. For example, Figure 1 compares the fractional frequency stability σ_z (or equivalently MOD$\sigma_y(\tau)$) for pulsars 1937+21, 1855+09, and J0437-4715 with that of a typical atomic clock that would contribute to TAI. Over timescales of a few years, J0437-4715 may be more stable than an atomic clock [4],[5],[6].

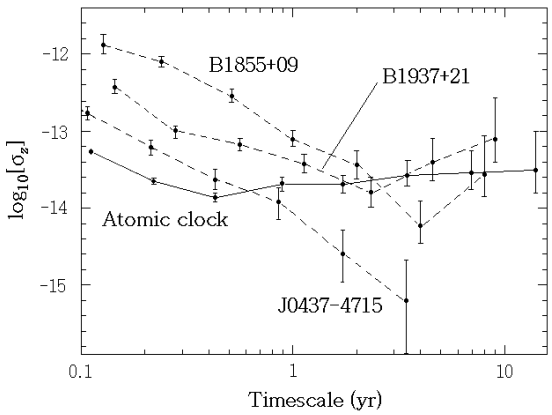

Fig. 1. Timing stability of radio signals from pulsars B1937+21, B1855+09, and J0437-4715, compared with that of an atomic clock.

To compare the stability of rotation-powered pulsar timing with other clocks, we give a plot of clock fractional frequency stabilities and compare them with the

frequency stability of pulsar B1937+21 in Figure 2. The stability of this pulsar is comparable to that of a commercial Cs clock after about 10^7 s of averaging. The good frequency stability provides a determination of position and velocity of the spacecraft better than by star tracking alone.

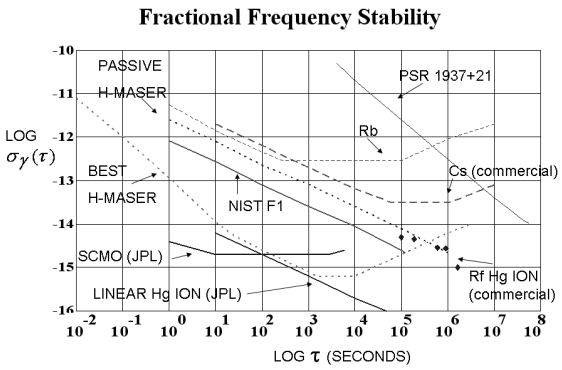

Fig. 2. Comparison of the frequency stability of pulsar PSR 1937+21 to other typical clock sources.

Pulsar signal shapes called 'profiles' are obtained by creating a data file of time-tagged, detected photons. Figure 3 shows the profile of X-ray signals detected by the USA satellite from the Crab pulsar, binned into time slots, and summed for about 10 minutes, assuming the detector is at the solar system barycenter. In practice the detector is in motion so the pulse period at the detector is Doppler shifted. For long integration times, a stable atomic clock is required for time-tagging. A pulse period is assumed and the time tags are folded into a single time interval equal to the period, with each photon being put into one of the bins into which the period has been divided. If the period is correct, one or more strong peaks will appear. If the Doppler frequency shift has not been correctly accounted for, the peaks in the pulse profile will be smeared into neighboring bins. Determining the period for which the peak-to-background counts are largest gives the detector's velocity relative to the assumed origin.

The phase of the peaks relative to the phase of the "true" profile at the barycenter then gives information about the component of the detector's displacement from the barycenter along the line of sight to the pulsar. Let $\mathbf{n}$ be a unit vector along the line of sight from the solar system barycenter to the pulsar, and $\mathbf{r}$ be the displacement of the detector from the barycenter. Then to a first approximation,

$$t_d - t_b = -\frac{\mathbf{n}\cdot\mathbf{r}}{c}\,, \qquad (1)$$

where t_d is the arrival time of the pulse at the detector and t_b is the arrival time of the same pulse at the barycenter. This equation shows the origin of an important source of error: if the celestial position $\mathbf{n}$ has too much uncertainty, an uncertainty in $\mathbf{r}$ will ensue no matter how good the timing is.

Figure 3 shows the profile of the Crab pulsar. The Crab is a young pulsar and one of the most powerful of the rotation-powered pulsars, and so tends to display frequency anomalies as the stellar material settles. This pulsar has the following characteristics:

- Right Ascension: 05:34:31.973 hr:min:sec;
- Declination: +22:00:52.06 deg:min:sec;
- period P = 33.08471603 ms;
- $\frac{dP}{dt} = -4.22765 \times 10^{-13}$;
- Pulse Profile: strong source with lots of background from the nebula.

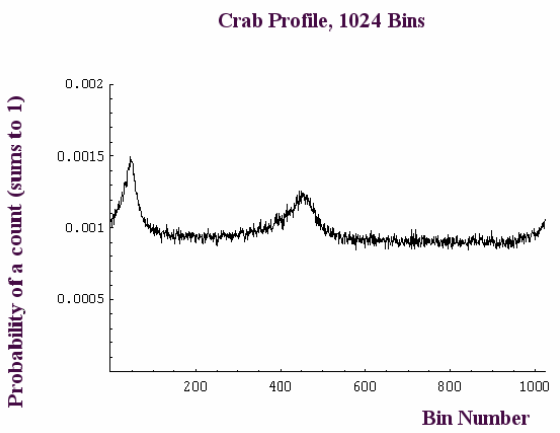

Fig. 3. Profile of the Crab pulsar.

In sum, a measurement consists of: time-tagging photon times of arrival; binning the data stream and measuring period (gives velocity); determining phase of arriving pulse relative to arrival phase at reference frame origin (gives position). In addition, the direction of the line of sight to the pulsar relative to spacecraft-fixed axes gives information about spacecraft attitude.

The pulse profile of the signal from the Crab is shown in Figure 3 in terms of the probability of receiving a count in one of the 1024 bins. One sees from this plot that the pulses do not show up strongly against the intense background. Also the noise in the profile is not intrinsic to the pulsar but arises from Poisson counting statistics. Time-tagged data for over a million photons were used to construct the profile in Figure 3.

3. Intrinsic Local Clock Noise

A model for uncertainty contributions to x-ray navigation, arising from local clock noise, has been developed under the following assumptions:

- The frequency noise is white; time noise is modelled by random walk with Gaussian statistics;
- The apparent pulsar period P is known at the local on-board clock (if not, then no pulse profile can be seen);
- The clock divides P up into N_b bins of size Δ (sec);

- Observations are conducted for N periods and counts are folded into the N_b bins;
- In each bin, the average count rate is described by a known pulse profile $R(t)$, with $R(t+P) = R(t)$;
- The edges of each bin during each cycle P wander due to random walk of the local clock;
- The intrinsic clock noise initializes at $t = 0$ and is modeled as white frequency noise, which is equivalent to random walk in phase or time.

In terms of this model of random walk in phase, it can be shown that the stability measure, Allan deviation, can be expressed as

$$\sigma_y(\tau) = \frac{\sigma_0}{\sqrt{\tau\Delta}}\,, \tag{2}$$

where σ_0^2 is the variance of the steps in the random walk that occur every Δ seconds, and τ is the averaging time.

Figure 4 illustrates the effect of white frequency noise. κ labels the bins: $\kappa = 1, 2, ...N_b$.

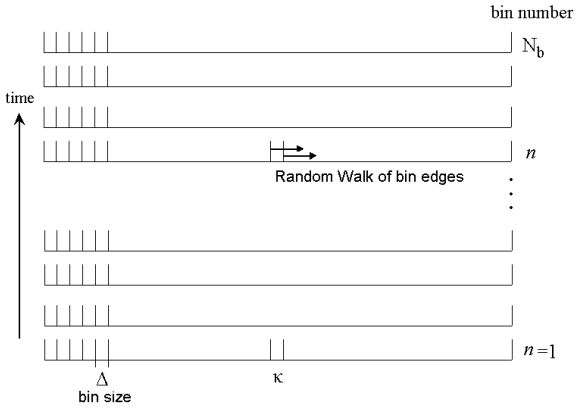

Fig. 4. White frequency noise of the on-board clock causes time random-walk of the edges of each κ time bin.

3.1 *Intrinsic Clock Noise Analysis*

The random walk in time affects the beginning and end of each κ^{th} time slot. Here w is a random walk in time of mean zero and variance σ_0 that occurs every Δ. Let the counting rate be

$$R(t) = R(t+P). \tag{3}$$

The times at the beginning and end of the (n,k) bin are respectively denoted by t_b, t_e. Then

$$t_b = (n-1)P + (\kappa-1)\Delta + \sum_{m=1,\tau=1}^{n-1,N_n-1} w_{m,\tau} + \sum_{\tau=1}^{\kappa-1} w_{n,\tau}; \tag{4}$$

$$t_e = (n-1)P + \kappa\Delta + \sum_{m=1,\tau=1}^{n-1,N_n-1} w_{m,\tau} + \sum_{\tau=1}^{\kappa} w_{n,\tau}. \tag{5}$$

Then the main contribution to the error in the counts C_κ in the κ^{th} bin, after performing appropriate ensemble averages, can be shown to be

$$\left\langle \delta C_\kappa^2 \right\rangle = \frac{N_b\sigma_0^2}{3} N^3 [R(\kappa\Delta) - R((\kappa-1)\Delta)]^2 + O(N^2). \tag{6}$$

The result can be compared to the estimated error in the κ^{th} bin from the Poisson statistics of the counts; that is, the counting statistics error is

$$\left\langle \delta C_\kappa^2 \right\rangle_{Poisson} = NR(\kappa\Delta)\Delta\,. \tag{7}$$

The difference $R(\kappa\Delta) - R((\kappa-1)\Delta)$ is simply related to

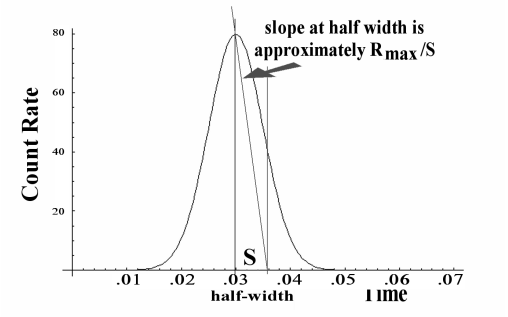

Fig. 5. Estimating the maximum slope of a pulse profile.

the slope of the pulse profile. We can obtain a crude estimate of the maximum slope–and hence the maximum intrinsic clock noise error–by examining the Gaussian pulse profile shown in Figure 5. If the maximum count rate is R_{max} and the half-width of the pulse is S, then the slope at the half-width is approximately R_{max}/S. This estimate could easily be off by a factor of 2 or so, which is however not significant in this analysis.

3.2 *White Frequency Noise Errors*

The ratio of error due to white frequency noise to error due to counting statistics is then approximately

$$r_\kappa = \sqrt{\frac{\langle \delta C_\kappa^2 \rangle}{\langle \delta C_\kappa^2 \rangle_{Poisson}}} = \sqrt{\frac{2}{3}} \frac{\sigma_0 \sqrt{N_b R_{max}\Delta}}{S} N. \tag{8}$$

As an example, use 1024 bins and the information about the Crab pulsar given above. Assume the pulse half-width is $\frac{1}{6}$ of the period, $P = 33$ ms, the average count rate $= 130$ counts/cycle, and $N = \frac{T}{P}$, where T is the total observation time. The result is expressed as a ratio of count error in a bin to count error arising from Poisson statistics:

$$r_\kappa(max) \simeq \sqrt{\frac{2}{3}} \frac{\sigma_0}{S} \sqrt{\frac{R_{max}}{P}} T \approx (1.3 \times 10^{-8}\text{sec}^{-1}) \times T. \tag{9}$$

The main result from this ratio is that for a reasonably stable clock, photon count errors arising from intrinsic clock noise are negligible compared to count errors arising from counting statistics (Poisson statistics). This shows that Poisson counting statistics are much more important than random walk in phase of a good atomic-clock signal source. Random walk in frequency can also be analyzed analytically but is not reported here.

4. Relativistic effects on clocks in space

Clocks in space are influenced by numerous relativistic effects. Fortunately most relativistic effects are very small and can be summed or superposed. At current levels of accuracy for space-qualified atomic clocks the effects can be grouped into three main types: second-order Doppler shifts, gravitational frequency shifts, and coordinate slowing (Shapiro time delay)[7] of the speed of electromagnetic waves that pass near a massive body. Doppler and gravitational frequency shifts are of order $1/c^2$ while the Shapiro time delay is of order $1/c^3$. Effects of order $1/c^4$ are negligible.

An imaginary atomic clock at the solar system barycenter, running at a conventional rate, is usually taken as a reference; such a clock is assumed to have zero velocity even though the velocity of the solar system relative to the cosmic microwave background radiation is known to be nearly 400 km/s. The second-order Doppler fractional frequency shift of a clock in space is then $-v^2/2c^2$ where v is the magnitude of the clock's velocity. If Φ_0 is the gravitational potential at the reference point and Φ the potential at the atomic clock, then the gravitational frequency shift is

$$\frac{\Delta f}{f} = \frac{\Phi - \Phi_0}{c^2}. \tag{10}$$

The Shapiro time delay requires corrections to Eq. 1; such corrections are currently only approximately included in many barycentering codes.

Atomic clocks in earth-bound orbit suffer from similar relativistic effects, but the reference point is then taken to be on earth's geoid. The average fractional frequency shift relative to such a reference is

$$\frac{\Delta f}{f} = -\frac{3GM_E}{2ac^2} + \frac{GM_E}{a_1c^2} + \frac{GM_EJ_2}{2a_1c^2} + \frac{\omega_E^2 a_1^2}{2c^2} \tag{11}$$

where a is the orbit semimajor axis, e is the orbit eccentricity, a_1 is earth's equatorial radius, G is the Newtonian gravitational constant, and M_E is the earth's mass. For an orbit comparable to that of the space station, $\Delta f/f \approx -3 \times 10^{-10}$. The frequency shift is dominated by time dilation, or the second-order Doppler shift. The effect on satellite clock time due to orbit eccentricity is

$$\Delta t = \frac{2\sqrt{GM_Ea}}{c^2} e \sin E + \text{const.} \tag{12}$$

Most of these effects are well-known in the context of GPS satellite clocks. For GPS satellite clocks, the first term in Eq. 11 ($\sim 10^{-10}$) is the actual effect on the clock of gravity and motion. The appearance of the semi-major axis of the orbit (a in the first term) reflects the dependence of the atomic clock frequency on orbital position. The second term affects the reference clocks on earth's surface ($\sim 10^{-10}$ due to earth's mass). The third term ($\sim 10^{-13}$) arises from earth's oblateness and affects earth-bound reference clocks. The last term is due to earth's rotation and also affects reference clocks.

An orbiting atomic clock provides proper time. There is a significant difference between proper time and the coordinate time provided by the reference. The difference must be carefully considered in establishing the times-of-arrival of pulsar photons.

The proper time of clock in low earth orbit could be converted with the aid of a GPS receiver, to GPS coordinate time, then to Terrestrial Time, then to Barycentric Coordinate Time if desired. Such transformations involve additional relativistic effects. For example, because earth's orbit about the sun is eccentric, conversion of Terrestrial Time to Barycentric time involves a correction of the form of Eq. 12 with M_e replaced by $M_\odot$, and with a and e representing the semimajor axis and eccentricity of earth's orbit and E the earth's eccentric anomaly.

5. Conclusion–Current Status

Navigation accuracies of the order of 10^2 meters may ultimately be possible, but a number of issues must be addressed. Reducing uncertainties that arise from celestial pulsar position errors is critical. Other clock noise and frequency drift errors, and clock time and synchronization errors affect the measurement of photon times-of-arrival and the transformations from terrestrial time to barycentric coordinate time. Instrumental noise and jitter also affect the time-of-arrival tags and require development of fast detectors and associated electronics. Additional relativistic clock effects from solar system bodies are important. Reducing uncertainties that arise from celestial pulsar position errors is critical. Increased counting rates are required before intrinsic reference clock noise becomes the cause of precision and accuracy limitations for x-ray navigation.

In sum, XNAV is an extremely challenging and interesting idea and promises to exploit the remarkable timing stability of the many rotation-powered pulsars that have been intensively studied by astronomers in the past three or four decades.

References

[1] Hanson, J. E., "Principles of X-ray navigation," doctoral dissertation, Stanford University (1996).

[2] Woodfork, D. W. II, K. F. Raquet. and R. A. Racca, "Use of X-ray pulsars for aiding GPS satellite orbit determination," ION 61st annual meeting, The Mitre Corporation & Draper Laboratory, 27-29 June 2005, Cambridge, MA.

[3] Sheikh, S. I., D. J. Pines, P. S. Ray, K. S. Wood, M. N. Lovellette, and M. T. Wolf, "The use of X-ray pulsars for spacecraft navigation," 14th AAS/AIAA Space Flicht Mechanics Conference, February 1004, AAS 04-109.

[4] Davis, M. M., Taylor, J. H., Weisberg, J. M., and Backer, D. C., *Nature* **315**, 1985, pp. 547-550.

[5] Matsakis, D. N., Taylor, J. H., Eubanks, T. M., and Marshall, T., A statistic for describing pulsar and clock stabilities, Astron. Astrophys ., 326, 924-928, (1997).

[6] Lorimer, D. R., "Binary and millisecond pulsars," http://relativity.livingreviews.org/Articles/lrr-2005-7.

[7] Shapiro, I. I., Phys. Rev. Letts. **13**, 789 (1964).